Radioactivity and lung cancer—mathematical models of radionuclide deposition in the human lungs

Robert Sturm

Institute of Physics and Biophysics, Department of Material Science and Physics, University of Salzburg, Salzburg, Austria

ABSTRACT

The human respiratory tract is regarded as pathway for radionuclides and other hazardous airborne materials to enter the body. Radioactive particles inhaled and deposited in the lungs cause an irradiation of bronchial/alveolar tissues. At the worst, this results in a malignant cellular transformation and, as a consequence of that, the development of lung cancer. In general, naturally occurring radionuclides (e.g., ^{222}Rn, ^{40}K) are attached to so-called carrier aerosols. The aerodynamic diameters of such radioactively labeled particles generally vary between several nanometers (ultrafine particles) and few micrometers, whereby highest particle fractions adopt sizes around 100 nm. Theoretical simulations of radioactive particle deposition in the human lungs were based on a stochastic lung geometry and a particle transport/deposition model using the random-walk algorithm. Further a polydisperse carrier aerosol (diameter: 1 nm–10 μm, $\rho \approx 1$ g cm^{-3}) with irregularly shaped particles and the effect of breathing characteristics and certain respiratory parameters on the transport of radioactive particles to bronchial/alveolar tissues were considered. As clearly shown by the results of deposition modeling, distribution patterns of radiation doses mainly depend on the size of the carrier aerosol. Ultrafine (< 10 nm) and large (> 2 μm) aerosol particles are preferentially deposited in the extrathoracic and upper bronchial region, whereas aerosol particles with intermediate size (10 nm–2 μm) may penetrate to deeper lung regions, causing an enhanced damage of the alveolar tissue by the attached radionuclides.

KEY WORDS Radionuclides; Carrier aerosol ; Monte Carlo model; Stochastic lung geometry

J Thorac Dis 2011;3:231-243. DOI: 10.3978/j.issn.2072-1439.2011.04.01

Introduction

In the past inhalation of radionuclides and its health effects were mainly studied for industrial workers (1-5), although they may additionally concern the general public in the case of exposure to environmental radon or unintentional release of radioactive material from industrial operations (5). Particularly in the 1950s and 1960s, nuclear weapons testing constituted as a further source, by which the population was confronted with highly hazardous radioactive elements that were taken up via the respiratory and the gastrointestinal pathway. Inhaled radionuclides irradiate tissues and cells of the respiratory tract. If they are cleared from the airways and alveoli via the blood or lymph vessels, they may also harm specific cellular components of extrapulmonary organs.

Inhalative uptake of airborne radionuclides by people breathing air that has been contaminated in any way mentioned above commonly depends on a large number of diverse factors. If radioactive elements occur in particulate rather than in gaseous form, which is realized by their attachment to ambient aerosol particles, the geometry, size, density, and hygroscopicity of the particulate matter have to be regarded as most important determinants controling the extent of radionuclide uptake. Numerous experimental studies (6-8) could demonstrate that the physical factors noted above as well as the mode of breathing (i.e., inspiration through the nose or mouth) and physiological breathing characteristics (tidal volume, breathing frequency) determine, whether inhaled radioactive substances are deposited in the respiratory tract or again exhaled. In the case of deposition, the properties outlined here additionally control the penetration depth of specific radionuclides, their sites of maximal deposition, their retention times or clearance rates, and their rates of absorption into the blood and subsequent translocation to adjacent tissues.

As soon as a particle attached by a radioactive element has

No potential conflict of interest.

Corresponding to: Robert Sturm, PhD. Institute of Physics and Biophysics, Department of Material Science and Physics, University of Salzburg, Hellbrunner Strasse 34, A-5020 Salzburg, Austria. Tel: +43-662-8044; Fax: +43-662-8044-150. E-mail: robert.sturm@sbg.ac.at

Submitted Jan 10, 2011. Accepted for publication Mar 25, 2011.
Available at www.jthoracdis.com

ISSN: 2072-1439 © 2011 Pioneer Bioscience Publishing Company. All rights reserved.

deposited on the epithelial surface of the respiratory tract, it starts to unfold its unwholesome efficacy on the adjacent tissue. The grade of this impairment among other depends on the solubility of the radioactive isotopes adsorbed on the carrier aerosol. Regarding the development of lung cancer, specific progenitor cells of the epithelium and especially their DNA molecules represent preferential targets for α-, β-, or γ-radiation. Whilst α-particles and γ-rays are mainly responsible for the generation of single strand breaks (SSB) or double strand breaks (DSB), γ-rays (and x-rays) may additionally affect the base-strand bonds, and β-particles preferably attack the connections between two bases (9-13). Normally, point or cluster damages of the DNA molecule are restored with the help of various reparation mechanisms. A failure of this restoration may generally occur in two forms: first, DSBs of the DNA remain unrejoined, resulting in cytotoxic effects; second, DNA damages are repaired incorrectly, causing the development of mutations (14,15).

Due to the ubiquitous occurrence of progenitor cells radiation-induced cancers may develop in both the extrathoracic and thoracic region of the human respiratory tract. Regarding the extrathoracic air passages tumor types mainly include squamous cell carcinomas, nonsquamous, mainly undifferentiated carcinomas, adenocarcinomas, sarcomas, epidermoid carcinomas, and, in extremely rare cases, esthesioneuroblastomas (5,16). Preferential target tissues of cancer formation are situated in the posterior nose and the nasopharynx, but also the larynx and the glottis bear a valuable potential for the growth of site-specific tumors.

In the thoracic region (trachea not included) four major types of carcinoma may be distinguished (Figure 1): adenocarcinoma, large cell carcinoma, squamous cell carcinoma (epidermoid carcinoma), and small cell carcinoma (17,18). Highest probability of occurrence in the large airways may be attributed to the squamous cell carcinoma and the small cell carcinoma. In the bronchiolar epithelium and alveolar-interstitial tissues the number of malignant neoplasms originating from respective progenitor cells is thought to be significantly reduced with

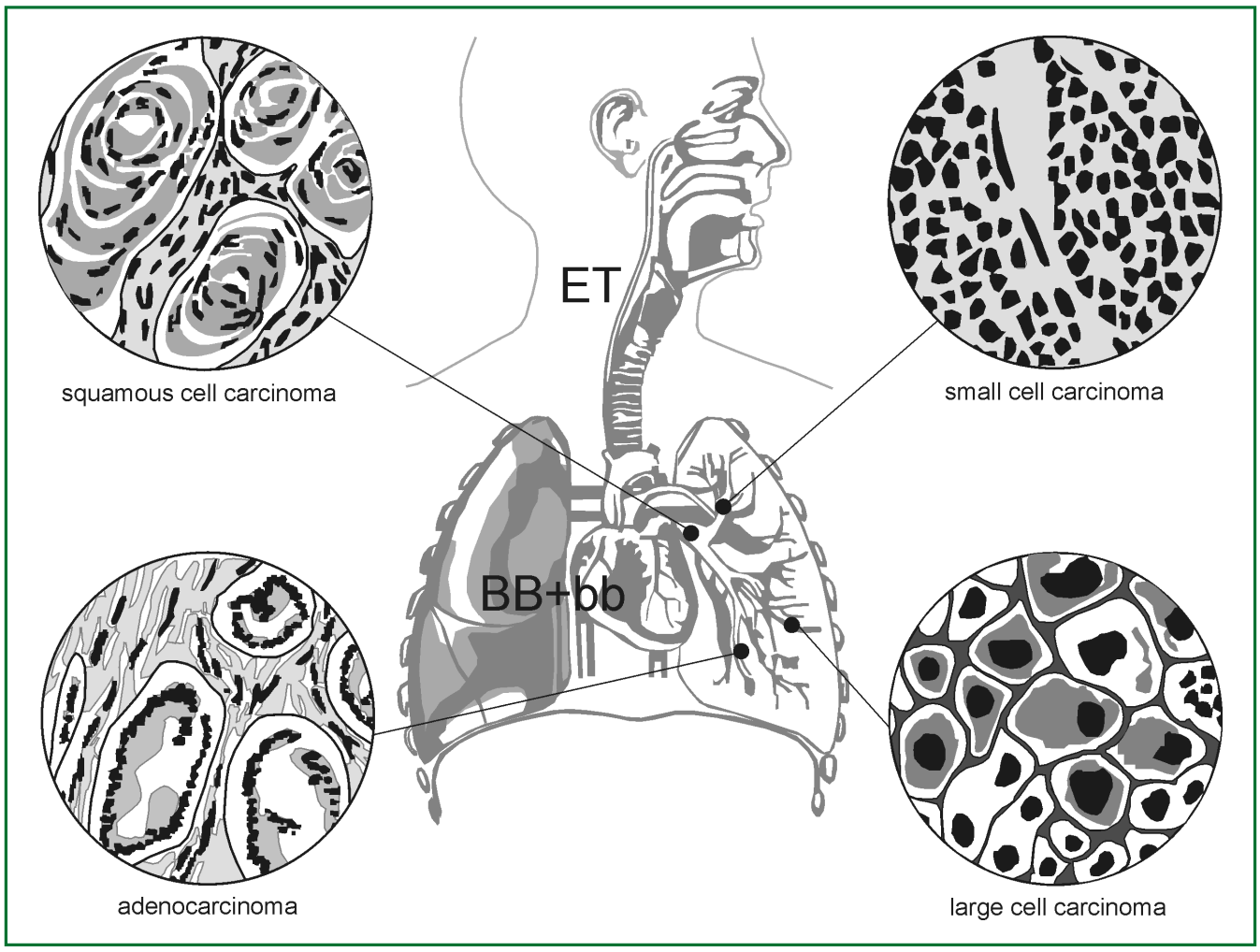

Figure 1. Main types of lung cancer and their preferential sites of formation in the human respiratory tract (5).

respect to that in the proximal lung region. However, in certain cases the percentage of tumors arising from the bronchioles may exceed 25 % (19), with adenocarcinoma being detected as preferred cancer type (20). The four major cancer types are distributed as follows (5): in nonsmokers about 30 % of diagnosed lung cancers are squamous cell carcinomas, 20 % are small cell carcinomas, 45 % are adenocarcinomas, and 5 % are large cell carcinomas. In smokers the proportion of squamous cell carcinomas may be enhanced to 50 %, whereas the proportion of adenocarcinoma may be decreased to about 25 %. Populations being affected by abnormal irradiation exhibit a disproportional increase of small cell carcinoma and a rather undifferentiated behavior of adenocarcinoma.

Mathematical approaches to radionuclide deposition in the human respiratory tract

Theoretical models of the lung structure

Current mathematical approaches of aerosol deposition in the human respiratory tract are founded upon lung architecture that is approximated by numerous sequences of straight cylindrical tubes (21-24), thereby forming a tree-like structure. According to the simplest morphometric models the branching network corresponds to a completely symmetrical tree structure, within which all airways of a given lung generation are characterized by identical geometric parameters (lengths, diameters, branching and gravity angles). As a consequence of this assumption, pathways leading from the trachea to the closing alveolar sacs show no variation in length (21). These properties, however, differ significantly from a realistic lung structure, where airway tubes belonging to a specific lung generation are characterized by partly considerable morphometric variations (intrasubject variability). To account for the intrasubject variability of airway morphometry in an appropriate way, symmetric models of the lung structure have been successively replaced by partly asymmetric or probabilistic approaches. Here, generation-specific variations of airway geometry are based upon statistical computations of respective morphometric datasets (25,26). Most currently, natural occurrence of the branching airway system has been approximated by a stochastic model of the whole human tracheobronchial tree (27). Morphometric data, upon which the stochastic approach is founded, originate from the comprehensive measurements published by Raabe et al. (28) and Haefeli-Bleuer and Weibel (29).

Stochastic transport and deposition model

The stochastic model predicting particle transport and deposition in the respiratory tract is based upon the random-walk of inhaled particles through a realistic airway branching structure. This principle is simply realized by randomly selecting a sequence of airways for each individual particle, whereby the geometry of single segments is varied according to the way described in the last section. At each bifurcation, the decision of the particle to enter either the major or the minor daughter airway is also randomly determined with the help of respective air-flow distributions, assuming that flow splitting is proportional to distal volume (30). As a main feature of the stochastic approach, estimation of particle deposition in a given airway is regarded to reflect the average deposition behavior of many (e.g., 10,000) particles. In order to appropriately handle a high number of deposition events, statistics obtained from the Monte-Carlo method are additionally improved by application of the statistical weight technique. Here, deposition of a particle in a given airway is simulated by decreasing its statistical weight instead of completely terminating its path. Hence, the particle continues its path through the lung structure with reduced statistical weight. The contribution of an individual deposition event to overall deposition in a specific lung generation is determined by multiplying the actual statistical weight of the particle with the site-specific deposition probability.

Particle deposition in individual airways due to various deposition forces is computed by using analytical deposition equations (23,24,31) which are valid for straight cylindrical tubes and spherical spaces (Table 1). Generally, three deposition mechanisms, i.e., Brownian motion, inertial impaction, and gravitational settling, are distinguished. Regarding particle deposition forced by Brownian motion, the related empirical equation outlined by Cohen and Asgharian (32), which considers an increase in deposition in the upper bronchial airways due to developing flow, is used additionally to the standard formulae. For the computation of particle deposition in more peripheral airway tubes, the respective diffusion equation proposed by Ingham (33) is applied. Deposition of particles in the upper airways caused by inertial impaction includes possible accumulation of particulate matter in the trachea (generation 0) due to turbulent flow (laryngeal jet) by the use of correction factors that are added to the respective standard equation. Regarding the estimation of extrathoracic deposition efficiencies, expressing the ability of nasal and oral airways to filter inspired particulate material, empirical equations were derived either from in vivo measurements (34) or from collected experimental data (35).

For transport and deposition calculations all bronchial airway lengths and diameters are routinely scaled down to a functional residual capacity of 3300 ml, whereby a constant linear scaling factor is used (5). The additional air volume produced by inhalation (tidal volume) does not cause a geometric modification among the bronchial airways, but is fully compensated by an isotropic increase of the alveolar diameter.

Table 1. Basic formulae for computation of particle deposition in cylindrical tubes and spherical spaces (23,24).

Mechanism	Equation(s), Variables	Coefficients
	Cylindrical Tubes	
Brownian motion	$p_d = 1 - \Sigma\, a_i exp(-b_i x) - a_4 exp(-b_4 x^{2/3})$	$a_1 = 0.819$, $b_1 = 7.315$
	$x = LD/2R^2v$	$a_2 = 0.098$, $b_2 = 44.61$
	D…diffusion coefficient	$a_3 = 0.033$, $b_3 = 114.0$
	R…radius of the tube	$a_4 = 0.051$, $b_4 = 79.31$
	L…length of the tube	
	v…mean flow velocity	
Sedimentation	$p_s = 1 - exp[-(4gC\rho r^2 L\, cos\phi)/(9\pi\mu Rv)]$	----------
	g…acceleration of gravity (9.81 m s^{-2})	
	ϕ…angle of tube relative to gravity	
	ρ…density of the particle	
	C…Cunningham slip correction factor	
	r…radius of the particle	
	μ…viscosity of the fluid	
Inertial impaction	$p_i = 1 - (2/\pi)\, cos^{-1}(\Theta St) + (1/\pi)\, sin$	----------
	$[2\, cos^{-1}(\Theta St)]$ for $\Theta St < 1$	
	$p_i = 1$ for $\Theta St > 1$	
	Θ…branching angle	
	St…Stokes number	
	Spherical spaces (uniform distribution of particles in the air, ideal alveolar mixing)	
Brownian motion	$p_d = 1 - (6/\pi^2)\, \Sigma\, (1/n^2)\, exp(-Dn^2\pi^2 t/R^2)$	----------
	n runs from 1 to ∞	
	D…diffusion coefficient	
	t…time	
	R…alveolar radius	
Sedimentation	$p_s = 0.5(u_s t/2R)\, [3 - (u_s t/2R)^2]$ if $t < 2R/u_s$	----------
	$p_s = 1$ if $t \geq 2R/u_s$	
	u_s…settling velocity	

Transport and deposition of nonspherical particles

Analytical equations predicting particle deposition in the human respiratory tract are based upon the simple hypothesis that all particles inhaled from the ambient atmosphere have ideal spherical shapes. However, this ideal geometry is limited to a low number of aerosol categories that may be found in nature or emanate from anthropogenic processes. Most particle types, above all those originating from industrial processes, are characterized by nonspherical (e.g., fibrous or disk-like) shapes. In some cases, they may also form irregularly shaped aggregates that consist of a high number of randomly arranged spherical or nonspherical components (36). Due to the tendency of radionuclides to be adsorbed on particles with large surface areas (e.g., mining dusts), the problem of aerosol particle geometry has to find increased consideration in respective transport and deposition models.

A theoretical approach to irregular particle shapes is the computation of the aerodynamic diameter (mobility diameter for ultrafine particles), d_{ae}, which denotes the diameter of a unit-density sphere with identical aerodynamic characteristics as the nonspherical particle of interest. In mathematical respects, this parameter is commonly expressed by the simple formula (37,38)

$$d_{ae} = d_{ve}\,[(1/\chi)(\rho_p/\rho_0)(Cd_{ve}/Cd_{ae})]^{0.5}, \quad (1)$$

where d_{ve} represents the volume-equivalent diameter (i.e., the diameter of a sphere with exactly the same volume as the investigated particle) and χ the dynamic shape factor, whilst ρ_p and ρ_0 denote the density (g cm^{-3}) of the particle and unit-density (1 g cm^{-3}). The remaining variables Cd_{ve} and Cd_{ae} are the so-called Cunningham slip correction factors for spheres

with diameters d_{ev} and d_{ae}, respectively. For oblate (i.e., disk-like) or prolate (i.e., fibrous) geometry the dynamic shape factor χ generally adopts values greater than 1 and, in the case of particles with highly irregular geometries, also values around 15 (37). The Cunningham correction factors may be neglected for particles that are transported in the continuum regime (i.e., particles with diameters greater than 1 μm), because they uniformly take values around 1. In the slip-flow regime, which represents the dominant aerodynamic environment for particles smaller than 1 μm and especially for ultrafine particles (< 100 nm), the factors become significant determinants with regards to the calculation of d_{ae}, thereby following an exponential increase with decreasing particle size. Mathematical formulation of Cd_{ve} and Cd_{ae} among other includes the mean free path length of oxygen molecules which depends upon temperature.

Results of theoretical deposition calculations and their experimental validation

Theoretical deposition simulations described in the following sections are based on the assumption that radionuclides have been attached to inhalable particulate matter and are not taken up in gaseous form. Subsequent to their deposition on the epithelial surface of the human respiratory system radionuclides (α-emitters) may be separated from the carrier aerosol by recoil processes, resulting in the emission radiation towards the epithelial tissues (see above). For theoretical calculations, aerodynamic diameters of the carrier particles were varied from 0.001 μm to 10 μm. Additionally, a uniform density of 1 g cm^{-3} was assumed. For an appropriate comparison of theoretical predictions with results obtained from experiments (39), the following breathing conditions were applied: 1) 500 cm^3 tidal volume, 4 s breathing cycle period (250 cm^3 s^{-1} flow rate), 2) 1000 cm^3 tidal volume, 8 s breathing cycle period (250 cm^3 s^{-1} flow rate), 3) 1500 cm^3 tidal volume, 4 s breathing cycle period (750 cm^3 s^{-1} flow rate), 4) 1000 cm^3 tidal volume, 16 s breathing cycle period (125 cm^3 s^{-1} flow rate). All four breathing scenarios were applied assuming 1) particle transport through the oral airways and 2) particle transfer via the nasal path.

Total deposition of particles attached with radionuclides in the human respiratory system

Generally, the dependence of total deposition on aerodynamic particle diameter is expressed by a U-shaped function with its minimum being localized at particle sizes of ≈ 0.5 μm. The maxima of the curve are situated at the margins of the logarithmic diameter scale (Figure 2). Regarding breathing scenario 1, the computed total deposition curve is marked by a wide minimum ranging from $d_{ae} \approx 0.1$ to $d_{ae} \approx 1$ μm (Figure 2A). The lowest value calculated for total deposition under the given conditions amounts either to 9 % (mouth breahting) or to 14 % (nose breahting). Total deposition of nanoparticles (0.001 μm) varies between 82 % (mouth breathing) and 93 % (nose breathing), whilst respective deposition of largest inhalable particles (10 μm) takes values of 73 % (mouth breathing) and 98 % (nose breathing).

An increase of the tidal volume but maintenance of the flow rate (breathing scenario 2) causes an enhancement of total deposition. In addition, the related deposition curve tends to change from U-shape with wide minimum into V-shape with narrow minimum (Figure 2B). At the minimum (d_{ae} = 0.5 μm), total deposition adopts values of 14 % (mouth breathing) and 19 % (nose breathing). Nanoparticles are deposited with amounts of 93 % (mouth breathing) and 100 % (nose breathing), whilst largest inhalable particles exhibit deposition values of 87% (mouth breathing) and 100 % (nose breathing).

By further increasing the tidal volume and additionally elevating the flow rate (breathing scenario 3) a noticeable effect on the velocity of the air flowing through the bronchial and alveolar system may be recognized. This results in an intensification of large particle deposition but a lessening of ultrafine particle deposition (Figure 2C). A contrary effect is observable by decreasing the flow rate to a certain extent (breathing scenario 4; Figure 2D).

Regional deposition of radioactively loaded particles

The human respiratory tract may be subdivided into three main regions, namely the extrathoracic region (ET), being subdivided into the oral route (mouth cavity, oropharynx, larynx) and the nasal route (nose, nasopharynx, larynx), the bronchial/bronchiolar region (BB+bb), representing the airway system, and the alveolar region (AI) (5).

Concerning the deposition of radioactive particles with variable size in the extrathoracic passages, deposition curves are again characterized by more or less perfect U-shapes (Figure3). According to breathing scenario 1 particles with d_{ae} ranging from 0.07 μm to 1 μm are not characterized by a measureable deposition in the oral path, whereas their deposition in the nasal airways varies between 7 and 15 %. This discrepancy between oral and nasal deposition is also recognizable for ultrafine and large particles. For particles with d_{ae} = 0.001 μm nasal deposition efficiency exceeds that of the mouth by a factor of 2.4 (34 % *vs* 82 %), whereas particles with d_{ae} = 10 μm exhibit a nasal deposition that exceeds oral deposition by a factor of 2.7 (32 % *vs* 86 %; Figure 3A). An increase of the tidal volume and maintenance of the flow rate (breathing scenario 2) has only negligible effects on the deposition curves (Figure 3B). Enhancement of the flow rate (breathing scenario 3) does not cause a remarkably change of intermediate-sized particle deposition with respect to breathing scenario 1. In contrast, large particles exhibit a partly dramatic

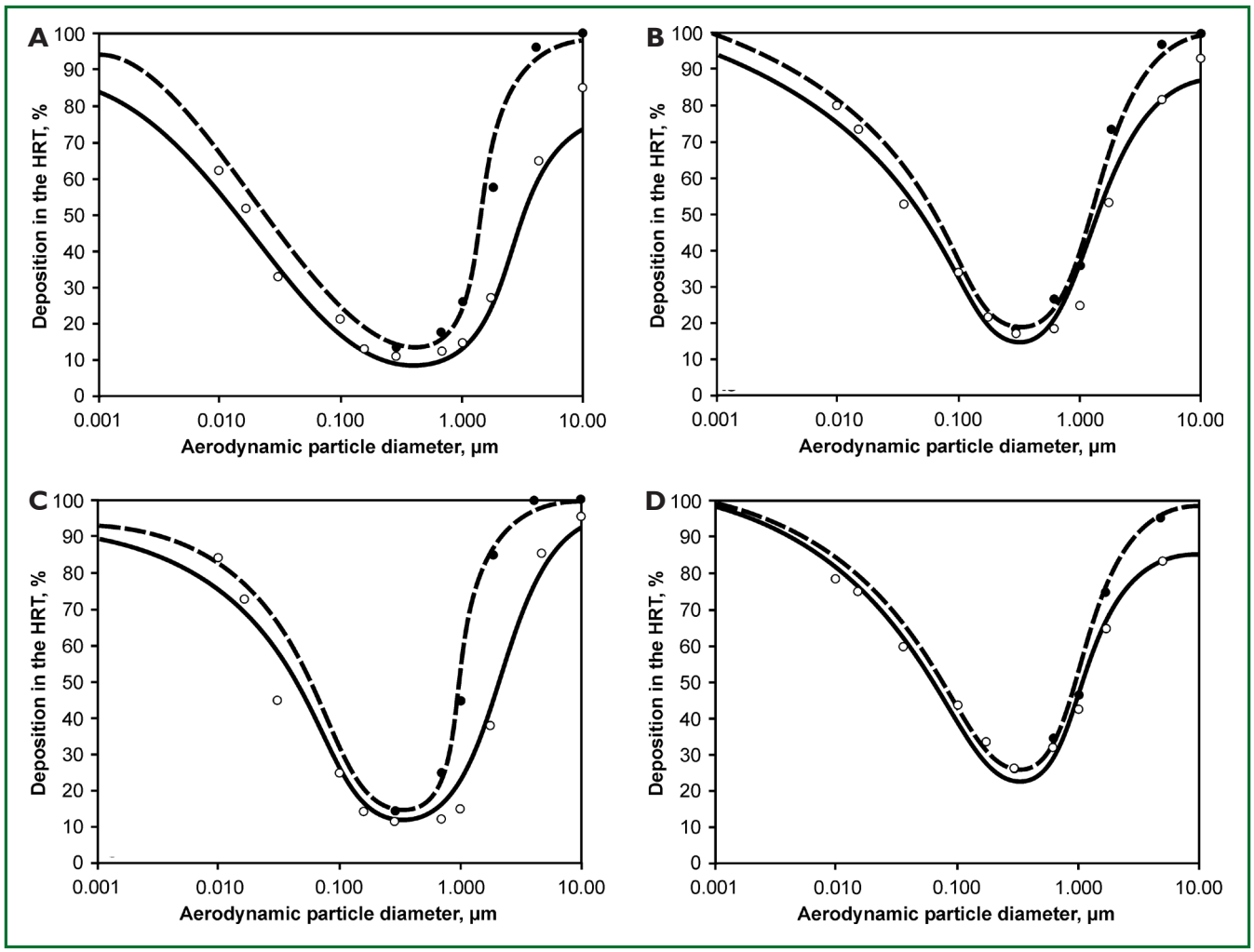

Figure 2. Total deposition of variably sized particles in the human respiratory tract. Whilst deposition curves represent theoretical predictions, plotted circles mark respective results from experiments (solid line/open circle: mouth breathing; dashed line/full circle: nasal breathing); A. Tidal volume: 500 cm^3, breathing cycle length: 4 s, flow rate: 250 cm^3 s^{-1}; B. Tidal volume: 1000 cm^3, breathing cycle length: 8 s, flow rate: 250 cm^3 s^{-1}; C. Tidal volume: 1500 cm^3, breathing cycle length: 4 s, flow rate: 750 cm^3 s^{-1}; D. Tidal volume: 1000 cm^3, breathing cycle length: 16 s, flow rate: 125 cm^3 s^{-1} (39).

increase in deposition (10 µm: 45 % in mouth, 96 % in nose), whilst ultrafine particles deposit in the extrathoracic passages with reduced efficiencies (1 nm: 23 % in mouth, 48 % in nose; Figure 3C). By reducing the flow rate (breathing scenario 4), large particle deposition is again subject to a decrease, and ultrafine particle deposition tends to a maximum (Figure 3D).

The main difference between extrathoracic and bronchial particle deposition consists in the circumstance that particles inhaled through the mouth are more effectively accumulated in the bronchial tubes than particles inhaled through the nose (Figure 4). The graphs of Figure 4 reveal phenomena differing in some parts from those introduced above. In general, deposition based on oral breathing varies between 3 % and 60 %, whilst deposition following the breathing through the nose exhibits values between 2 % and 20 %. Increase of the tidal volume but maintenance of the flow rate causes an increase of ultrafine and large particle deposition (Figure 4B). Accumulation of particles with intermediate sizes remains unaffected. Due to the increase of the flow rate (breathing scenario 3) ultrafine particles are subject to an enhanced collision with the bronchial walls (Figure 4C). By decreasing the flow rate (breathing scenario 4), deposition of large particles is enhanced again, thereby partly exceeding the respective accumulation efficiency of ultrafine particles (Figure 4D).

Deposition of radioactive particles in the alveoli is commonly expressed by bimodal functions (Figure 5) that are characterized as follows: (i) Deposition maxima are recognizable for d_{ae} = 0.04 µm and d_{ae} = 2-3 µm, whereas minimal deposition is given for

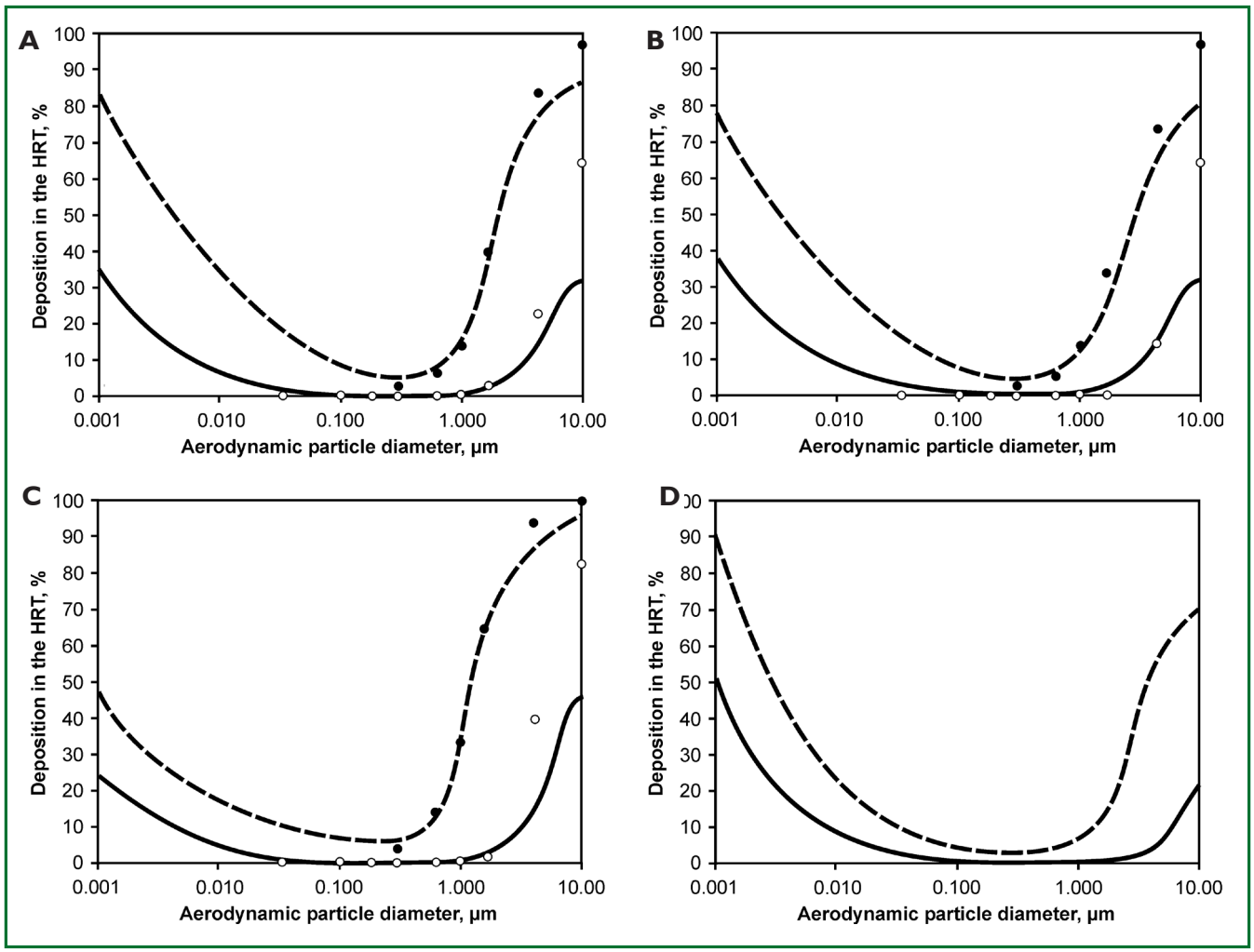

Figure 3. Extrathoracic deposition of particles with different aerodynamic diameters. For detailed descriptions of symbols, lines, and breathing setups presented in graphs A to D see caption of Figure 2.

particles with intermediate sizes (≈ 0.5 µm) and, for nano-scale and large particles; (ii) Alveolar particle deposition emanating from oral breathing is higher than deposition following breathing through the nose. In general, alveolar deposition for nano-scale and large particles ranges from 1 % to 18 % and that for intermediately sized particles from 3 % to 19 %. Depending on the selected breathing scenario the left maximum adopts values between 16 % and 55 %, whilst values for the right maximum range from 14 % to 52 %. Enhancement of the tidal volume (breathing scenario 2; Figure 5B) is accompanied by an alveolar deposition that proportionally increases for all particle sizes. A similar effect is attained by an increase of the flow rate (deposition scenario 3; Figure 5C), whereby the half-width of the peaks is subject to a reduction. Additionally, the left peak significantly exceeds the right one in height. A reduction of the flow rate (breathing scenario 4; Figure 5D) causes an increase of the right peak height and a respective decrease of the left one.

Radioactive particle deposition in single airway generations

Deposition of radioactive particles in single airway generations was computed under the assumption of mouth breathing. Relative deposition values were plotted from generation 0, corresponding with the trachea, to generation 20, representing the distal bronchioles (Figure 6). Deposition curves of 5 different particle sizes (0.001 µm, 0.01 µm, 0.1 µm, 1 µm, and 10 µm) were plotted together for the purpose of intercomparison. Generally, nano-scale particles (0.001 µm) exhibit high deposition in the proximal generations (4 %-10 %), which is subject to a dramatic decrease towards more peripheral airways. Particles with d_{ae} = 0.01 µm commonly deposit in the trachea with ≈ 1 % but increase their deposition continuously towards generation 15/16, where respective values range from 4.5 % to 7 %. From generation 16/17 onwards, deposition declines more or less rapidly. Aerosol particles with d_{ae} = 0.1 µm deposit

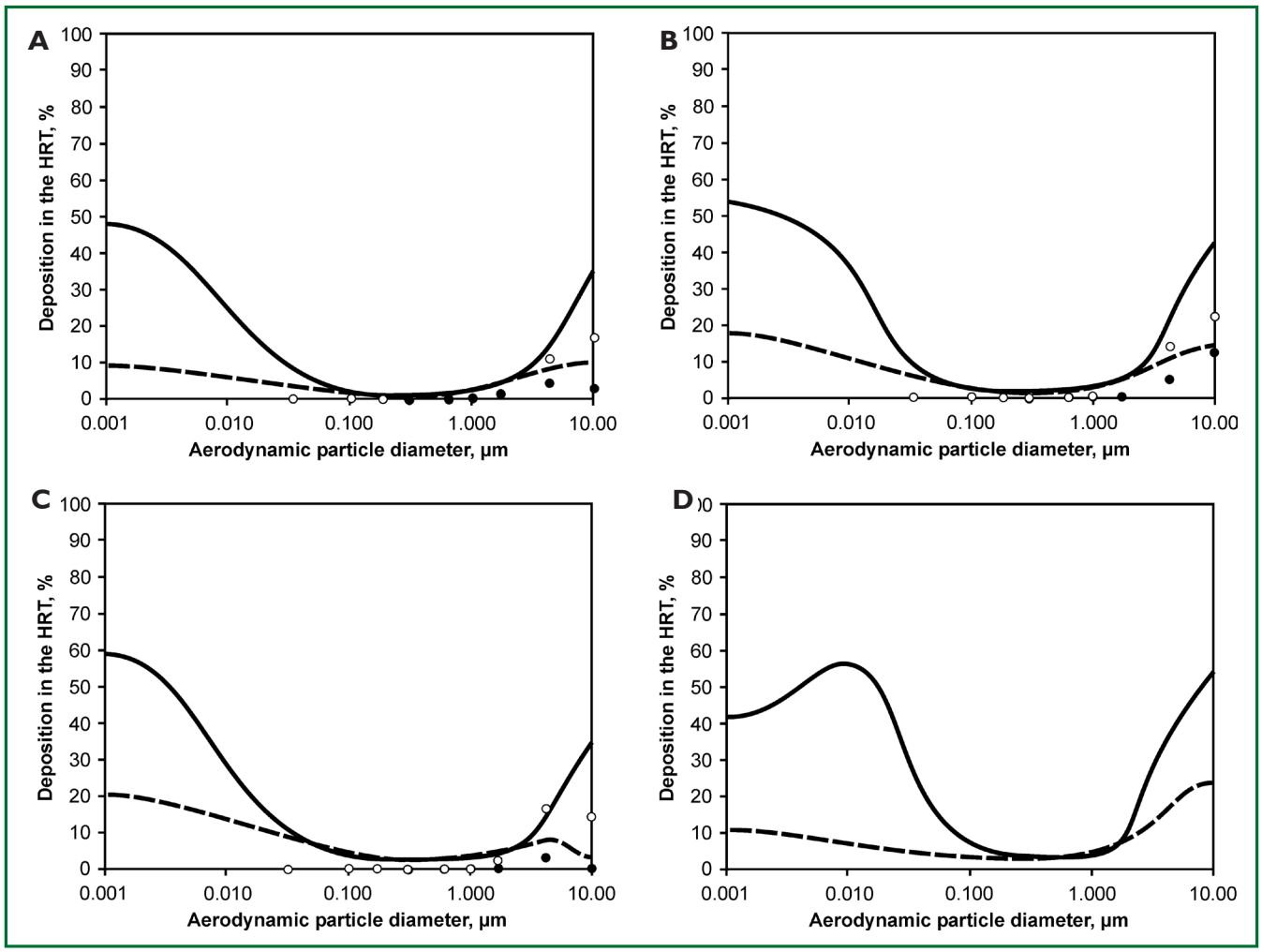

Figure 4. Bronchial deposition of particles with aerodynamic diameters ranging from 0.001 µm to 10 µm. For detailed descriptions of symbols, lines, and breathing setups presented in graphs A to D see caption of Figure 2.

with ≤ 1 % in the upper bronchial airways but increase their deposition towards the terminal and respiratory bronchioles, whSere it may finally range from 2 % to about 4.5 %. Concerning particles with d_{ae} = 1 µm, shape of the deposition pattern is similar to that described for the 0.1 µm particles. Deposition values of 1 µm particles are lower than those of 0.1 µm particles, thereby reaching maximal values of 3.7 %. Large particles (d_{ae} = 10 µm) show a small deposition maximum at airway generation 2/3, with respective deposition values ranging from 0.8 % to 2.3 % but a more remarkable one at airway generation 10/11 (deposition values: 0.8 % to 5 %). Towards more peripheral airways deposition continuously approaches to zero.

An enhancement of the tidal volume (breathing scenario 2; Figure 6B) results in a general increase in deposition which is most significant for intermediately sized particles. By elevating the flow rate (breathing scenario 3; Figure 6C) deposition curves of 0.001 µm and 0.01 µm particles are significantly changed in shape, indicating a displacement of maximal deposition values towards more distal airways. Deposition of 10 µm particles is subject to a general reduction that may be traced back to the increased extrathoracic deposition. Slow inhalation (breathing scenario 4; Figure 6D) again causes a partly dramatic increase of the generation-specific deposition values, now also affecting the 10 µm particles due to the enhanced efficacy of gravitational settling.

Discussion

From the theoretical results presented here several conclusions can be drawn that are essential to understand the behavior of particles that are attached by radioactive elements and inhaled into the human respiratory system. As generally determined from modeling calculations and related experiments, deposition sites and intensities of radioactively contaminated particulate

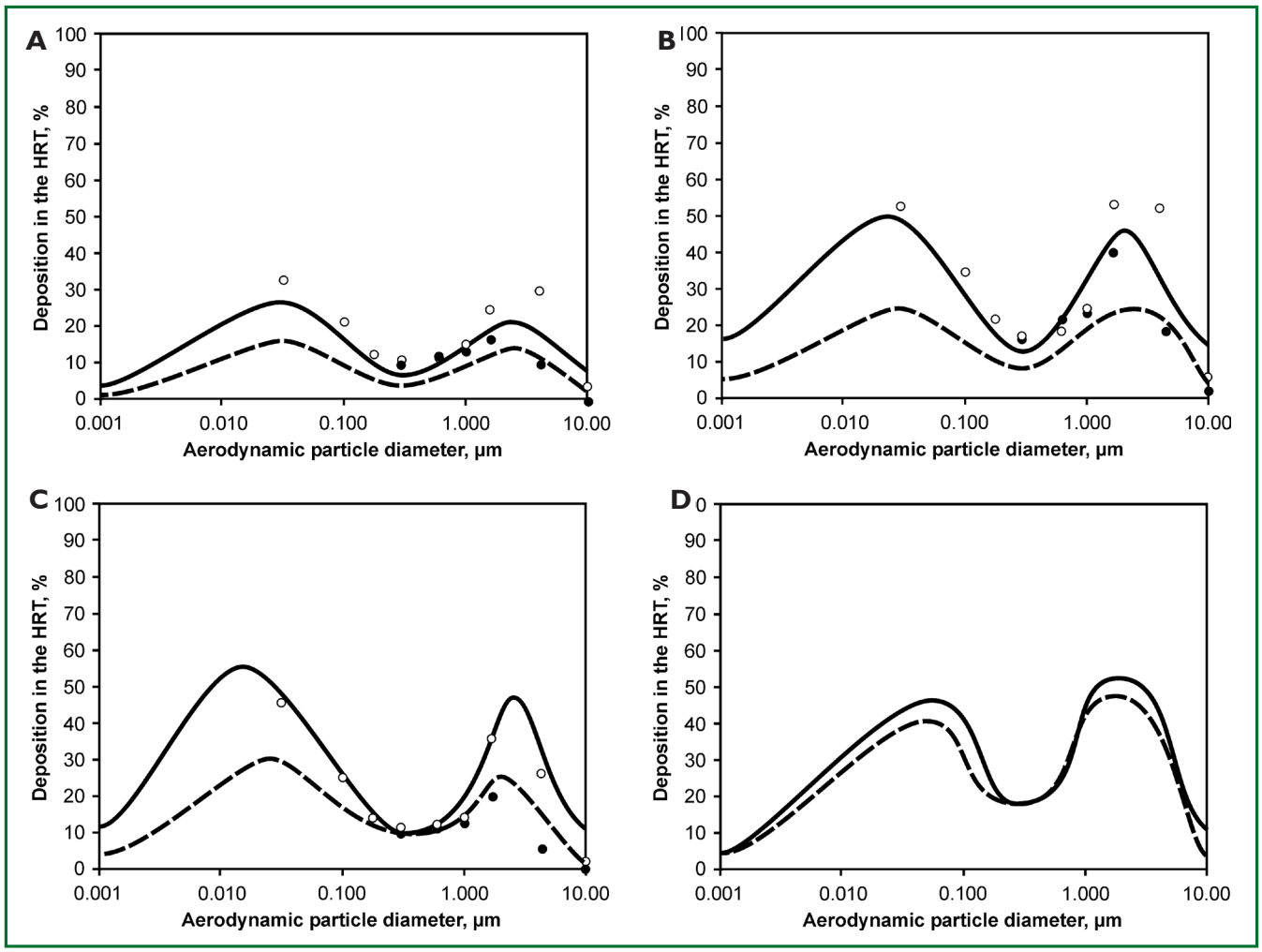

Figure 5. Alveolar deposition of variably sized particles. For detailed descriptions of symbols, lines, and breathing setups presented in graphs A to D see caption of Figure 2.

substances depend upon geometric (shape) as well as physical (e.g., density, electric charge) characteristics of single components being suspended in the ambient atmosphere. In order to consider both geometric and physical particle properties for transport and deposition computations, the aerodynamic diameter concept was established here and consequently applied to solve any questions which are of physical and medical interest (38). For the exemplary case of inhaled fibers previous investigations could demonstrate that fiber length has to be assumed as a minor determinant for deposition in the airways. On the other side, fiber diameter is of increased interest concerning this specific question (40,41). This results in the circumstance that very long (up to 100 µm) but extremely thin (much smaller than 1 µm) fibrous particles are characterized by high pulmonary penetration depths, leading to their significant accumulation in the alveolar spaces.

As revealed by the total deposition graphs, highest deposition efficiencies in the human respiratory system may be attested for those particles which either are very small, thereby commonly adopting diameters < 10 nm, or very large ($d_{ae} \approx$ 3-10 µm), whilst particles with intermediate sizes are to a significant extent expired from the respiratory tract again. Hence, highest danger for both the irradiation of epithelial cells and the malignant transformation of lung tissues emanates from aerosols containing either ultrafine or large particles (5,38). The reason for ultrafine and large carrier particles being deposited in high amounts in the respiratory tract is given by the deposition mechanisms affecting these specific particle classes. Whilst aerosols adopting diameters <100 nm undergo a remarkable deposition by Brownian diffusion (Table 1), particles with diameters >2 µm increasingly tend to be deposited by inertial impaction and gravitational settling (Table 1) (5,22,23,38,40). For intermediately sized aerosols the very specific phenomenon of pulmonary particle transport with low influence of deposition forces may be

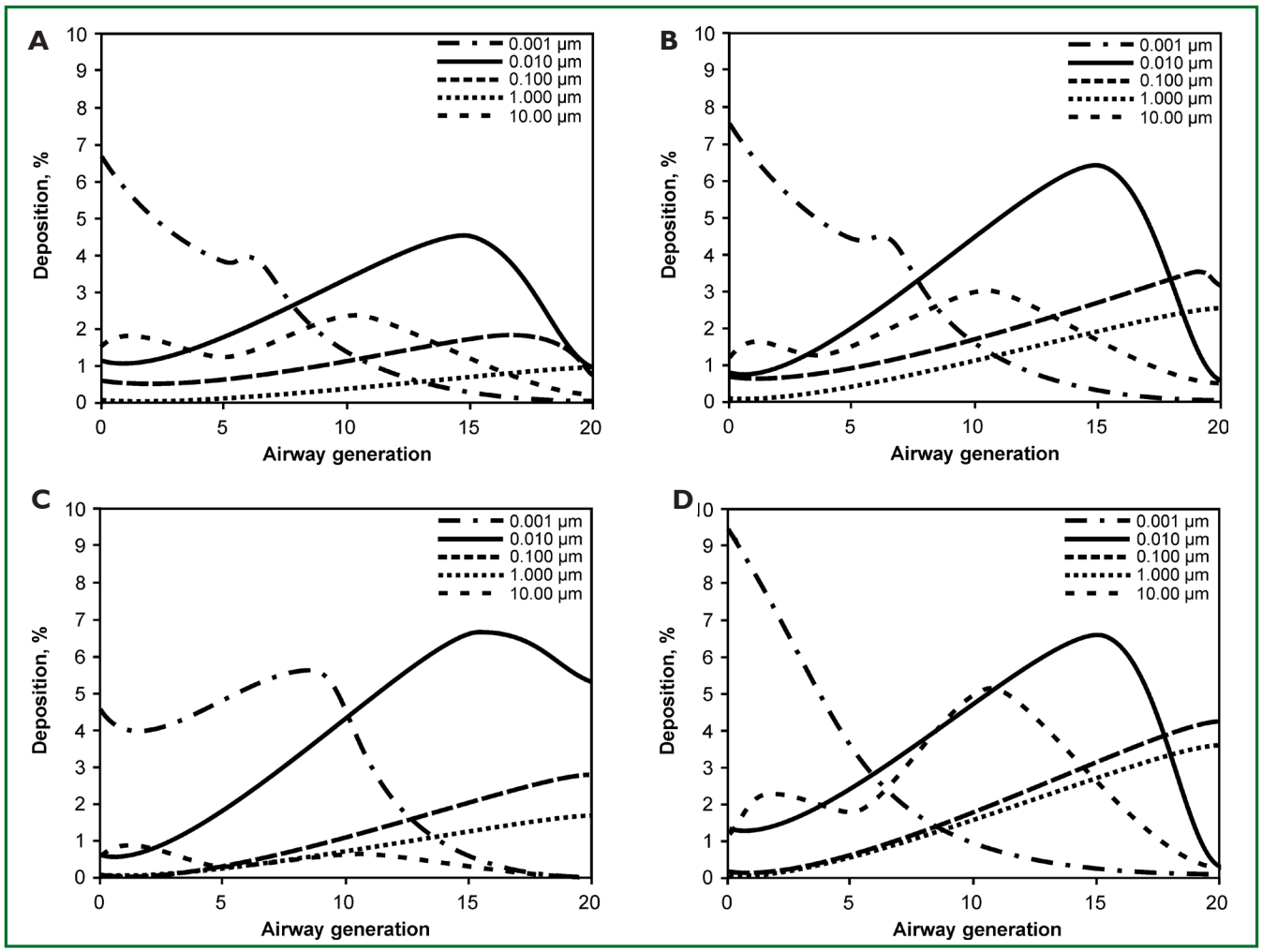

Figure 6. Generation-specific particle deposition for the exemplary case of mouth breathing; A. Tidal volume: 500 cm^3, breathing cycle length: 4 s, flow rate: 250 cm^3 s^{-1}; B. Tidal volume: 1000 cm^3, breathing cycle length: 8 s, flow rate: 250 cm^3 s^{-1}; C. Tidal volume: 1500 cm^3, breathing cycle length: 4 s, flow rate: 750 cm^3 s^{-1}; D. Tidal volume: 1000 cm^3, breathing cycle length: 16 s, flow rate: 125 cm^3 s^{-1}.

observed, resulting in the U-shaped total deposition functions presented in Figure 2.

Predictions of regional aerosol depositions clearly demonstrate that particles belonging to the two size categories mentioned above are preferably accumulated in the extrathoracic compartment and the upper bronchi, so that resulting carcinomas may be also localized at the respective sites. Intermediately sized particles, as far as being deposited in the human respiratory system, are chiefly accumulated in the distal bronchioles and the alveoli. As demonstrated by respective computations maximal alveolar deposition is restricted to rather small particle diameter intervals: particles with $d_{ae} \approx 0.04$ µm and $d_{ae} \approx 2$ µm have the alveolar region as their primary target and, thus, may cause enhanced cellular damage within this part of the lung. As already demonstrated in earlier investigations (40,41), distribution of cancer progenitor cells (e.g., goblet cells, brush cells, basal cells) differs the single compartments of the respiratory tract (Figure 7). Besides this significant factor also the airway surface area, serving for the computation of doses per cm^2 (doses per g) is subject to a remarkable change from proximal to distal lung regions, with alveolar surface being ≈ 3,500 times larger than bronchial and ≈ 600 times larger than bronchiolar surface (5). The consequence of this circumstance is a much higher probability of malignant transformation and carcinoma growth in the bronchi with respect to the alveoli. The predictions of regional particle deposition are confirmed by the generations-specific deposition plots, where 0.001 µm and 10 µm particles clearly tend to deposit in the proximal airway generations, whereas the remaining particle sizes studied here (0.01 µm, 0.1 µm, 1 µm) preferentially accumulate in intermediate to distal airway generations (40,41).

As undoubtedly illustrated in the deposition graphs of Figures 2-5, model predictions, especially those carried out for mouth breathing, are not always subject to a remarkable

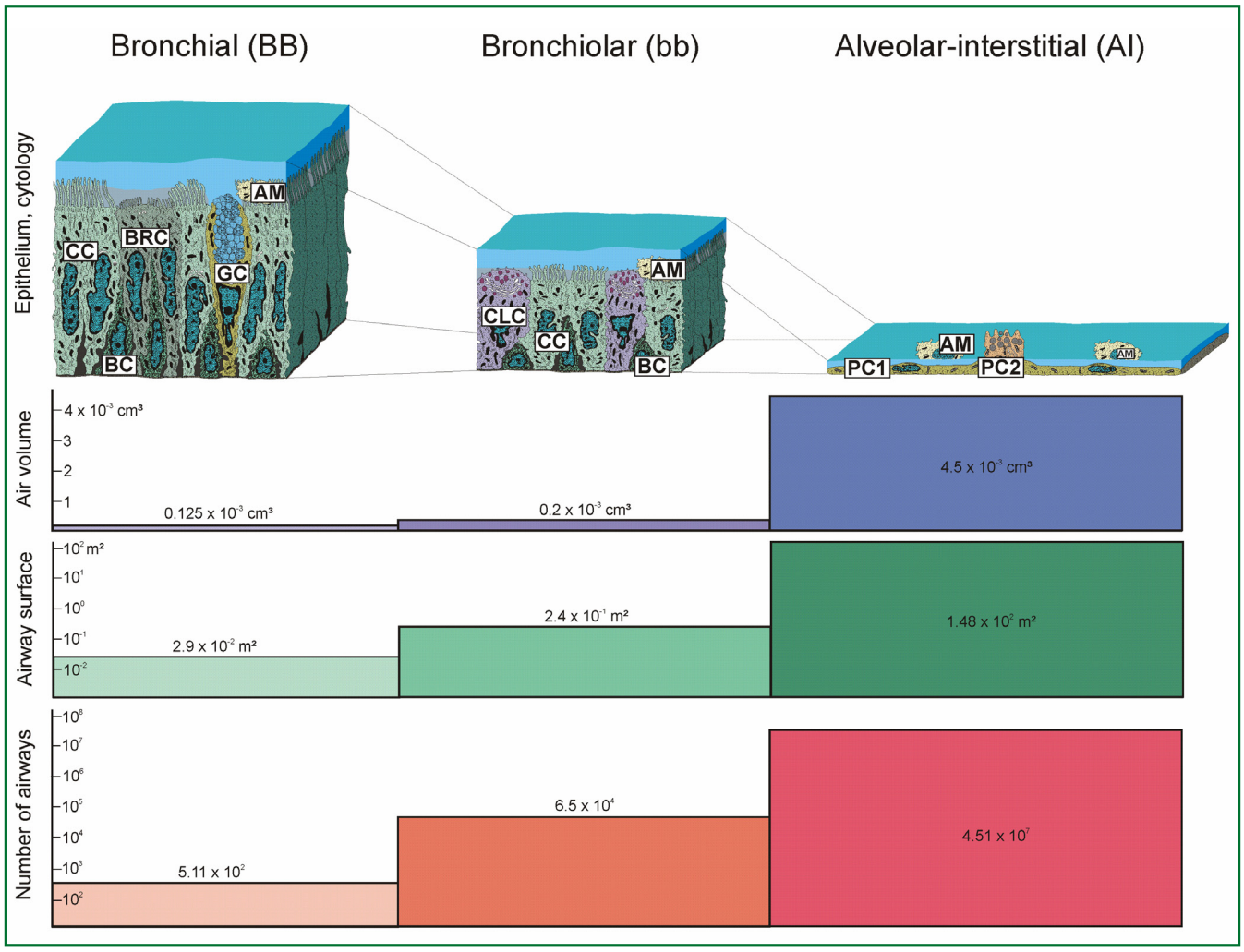

Figure 7. General cytology and main morphometric characteristics of the three thoracic compartments of the human respiratory tract (5). Abbreviations; AM: airway/alveolar macrophage; BC: basal cell; BRC: brush cell; CC: ciliated cell; CLC: Clara cell; GC: goblet cell; PC1: pneumocyte type 1; PC2: pneumocyte type 2.

correspondence with the respective experimental results. For large particles with d_{ae} > 1 μm, theoretical values for extrathoracic deposition (oral path) are significantly underestimated, whilst related values for bronchial deposition are partly much to high. The disagreement of extrathoracic deposition has its main reason in the use of empirical deposition formulae within the model (24) that allow the application of variable extrathoracic volumes but are not sensitive enough for the consideration of intersubject variabilities. Concerning the aspect of variable particle deposition in the mouth and oropharynx of test subjects, the model has to be significantly improved in future by the implementation of current numerical results.

Since the development of lung cancer has to be understood as a long-term process, specific clearance pathways of particulate matter deposited in the bronchial airways and alveoli have to be additionally considered in respective theoretical approaches. In general, large and very small particles chiefly accumulated in the extrathoracic region and proximal airways are preferably removed from the respiratory tract by fast clearance processes (mucociliary elevator), whereas particles with intermediate size and high ability to reach more distal lung parts (see above) are preferably subject to slow clearance mechanisms, significantly increasing their residence times in the bronchial and alveolar compartment (40,42,43).

An essential question concerns the possible effect of breathing mode on deposition. Therefore, the number of hazardous particles reaching the bronchial and alveolar region is remarkably declined by inhalation through the nose. Any change of breathing frequency and tidal volume may handicap deposition of one particle size category but favor deposition of the other. Due to its anatomical specificity including conchae dividing the inhaled air stream and sharply bent airways, the nose acts as a

highly efficient filtering system (5), with hazarduous particles being already accumulated in the extrathoracic region. Low breathing frequencies and high tidal volumes decelerate the inhaled air stream, thereby causing an increase of diffusion and sedimentation efficiency but a remarkable decrease of impaction efficiency (5,35,36). High breathing frequencies in combination with low tidal volumes result in a contrary effect.

By taking into account the modeling results presented in this contribution, it may be concluded that radioactively loaded particles that hit the epithelial walls of large airways have to be regarded as cause for the induction of squamous cell carcinoma and small cell carcinoma. On the other side, particles reaching the bronchiolar epithelium and alveolar-interstitial tissues may trigger the development of large cell carcinoma and adenocarcinoma. However, further theoretical and epidemiological studies will provide more detailed results and related medical perspectives in future.

References

1. Dagle GE, Sanders CL. Radionuclide Injury to the Lung. Env Health Persp 1984;55:129-37.
2. De Villiers AJ, Windish JP. Lung cancer in a fluorspar mining community. I. Radiation, dust and mortality experience. Brit J Ind Med 1964;21:94-109.
3. Wagoner JK, Archer VE, Lundin FE, Holaday DA, Lloyd JW. Radiation as the cause of lung cancer among uranium miners. N Engl J Med 1965;273:181-8.
4. Lorenz E. Radioactivity and lung cancer; a critical review of cancer in the miners of Schneeberg and Joachimstal. J Nat Cancer Inst 1941;5:1-5.
5. International Commission on Radiological Protection (ICRP). Human respiratory tract model for radiological protection. Publication 66. Oxford, GB: Pergamon Press; 1994.
6. Stahlhofen W, Gebhart J, Heyder J. Biological variability of regional deposition of aerosol particles in the human respiratory tract. Am Ind Hyg Assoc J 1981;42:348-52.
7. Heyder J, Gebhart J, Stahlhofen W, Stuck B. Biological variability of particle deposition in the human respiratory tract during controlled and spontaneous mouth-breathing. Ann Occup Hyg 1982;26:137-47.
8. Heyder J, Gebhart J, Scheuch G. Influence of human lung morphology on particle deposition. J Aerosol Med 1988;1:81-8.
9. Charlton DE, Nikjoo H, Humm JL. Calculation of initial yields of single- and double-strand breaks in cell nuclei from electrons, protons and alpha particles. Int J Rad Biol 1989;56:1-19.
10. Chatterjee A, Holley WR. Biochemical mechanisms and clusters of damage for high LET radiation. Adv Space Res 1992;12:33-43.
11. Goodhead DT, Munson RJ, Thacker J, Cox R. Mutation and inactivation of cultured mammalian cells exposed to beams of accelerated heavy ions IV. Biophysical interpretation. Int J Rad Biol 1980;37:135-67.
12. Goodhead DT, Nikjoo H. Track structure analysis of ultrasoft X-rays compared to high- and low-LET radiations. Int J Rad Biol 1989;55:513-29.
13. Nikjoo H, Goodhead DT, Charlton DE, Paretzke HG. Energy deposition in small cylindrical targets by monoenergetic electrons. Int J Rad Biol 1991;60:739-56.
14. Chapman JD, Doern SD, Reuvers AP, Gillespie CJ, Chatterjee A, Blakely EA, et al. Radioprotection by DMSO of mammalian cells exposed to X-rays and the heavy-charged particle beams. Rad Env Biophys 1979;16:29-41.
15. DeLara CM, Jenner TJ, Townsend KMS, Marsden SJ, O'Neill P. The effect of dimethyl sulfoxide on the induction of DANN double-strand breaks in V79-4 mammalian cells by alpha particles. Radiat Res 1995;144:43-9.
16. Batsakis JG. Tumors of the Head and Neck. Baltimore, MD: Williams & Wilkins; 1976.
17. Reznik-Schüller HM. The respiratory tract in rodents. In: HM Reznik-Schüller, editor. Comparative respiratory tract carcinogenesis. Boca Raton, FL: CRC Press; 1983. p. 79-93.
18. Yamamoto M, Shimokata K, Nagura H. Immunoelectron microscopic study of the histogenesis of epidermoid metaplasia in respiratory epithelium. Am Rev Resp Dis 1987;135:713-8.
19. Del Regato JA, Spjut HJ, Cox JD, editors. Cancer, diagnosis, treatment, and prognosis. St. Louis, Toronto, Princeton: The CV Mosby Company;1985.
20. Yamamoto T, Kopecky KJ, Fujikura T, Tokuoka S, Monzen T, Nishimori I, et al. Lung cancer incidence among Japanese A-bomb survivors, 1950-80. J Rad Res 1987;28:156-71.
21. Weibel ER. Morphometry of the human lung. Berlin, GER: Springer-Verlag; 1963.
22. Horsfield K, Dart G, Olson DE, Filley GF, Cumming G. Models of the human bronchial tree. J Appl Physiol 1971;31:207-17.
23. Yeh HC, Schum GM. Models of the human lung airways and their application to inhaled particle deposition. Bull Math Biol 1980;42:461-80.
24. Koblinger L, Hofmann W. Monte Carlo modeling of aerosol deposition in human lungs. Part I: simulation of particle transport in a stochastic lung structure. J Aerosol Sci 1990;21:661-74.
25. Soong TT, Nicolaides P, Yu CP, Soong SC. A statistical description of the human tracheobronchial tree geometry. Resp Physiol 1979;37:161-72.
26. Yu CP, Nicolaides P, Soong TT. Effect of random airway sizes on aerosol deposition. Am Ind Hyg Assoc J 1979;40:999-1005.
27. Koblinger L, Hofmann W. Analysis of human lung morphometric data for stochastic aerosol deposition calculations. Phys Med Biol 1985;30:541-56.
28. Raabe OG, Yeh HC, Schum GM, Phalen RF. Tracheobronchial geometry: human, dog, rat, hamster, LF-53. Albuquerque, NM: Lovelace Foundation; 1976.
29. Haefeli-Bleuer B, Weibel ER. Morphometry of the human pulmonary acinus. Anat Rec 1988;220:401-14.
30. Phillips CG, Kaye SR. On the asymmetry of bifurcations in the bronchial tree. Resp Physiol 1997;107:85-98.
31. Carslow HS, Jaeger HC. Conduction of Heat in Solids. Oxford, GB: Clarendon Press; 1959.
32. Cohen BS, Asgharian B. Deposition of ultrafine particles in the upper airways. J Aerosol Sci 1990;21:789-97.
33. Ingham DB. Diffusion of aerosol from a stream flowing through a cylindrical tube. J Aerosol Sci 1975;6:125-32.
34. Cheng KH, Cheng YS, Yeh HC, Guilmette RA, Simpson SQ, Yang Y, et al. In vivo measurements of nasal airway dimensions and ultrafine aerosol

deposition in the human nasal and oral airways. J Aerosol Sci 1996;27:785-801.
35. Stahlhofen W, Rudolf G, James AC. Intercomparison of experimental regional aerosol deposition data. J Aerosol Med 1989;2:285-308.
36. Davies CN. Particle-fluid interaction. J Aerosol Sci 1979;10:477-513.
37. Kasper G. Dynamics and measurement of smokes. I Size characterization of nonspherical particles. Aerosol Sci Technol 1982;1:187-99.
38. Sturm R, Hofmann W. A theoretical approach to the deposition and clearance of fibers with variable size in the human respiratory tract. J Hazard Mat 2009;170:210-21.
39. Heyder J, Gebhart J, Rudolf G, Schiller CF, Stahlhofen W. Deposition of particles in the human respiratory tract in the size range 0.005–15 μm. J Aerosol Sci 1986;17:811-25.
40. Sturm R. Deposition and cellular interaction of cancer-inducing particles in the human respiratory tract: Theoretical approaches and experimental data. Thoracic Cancer 2010;4:141-52.
41. Sturm R. Theoretical approach to the hit probability of lung-cancer-sensitive epithelial cells by mineral fibers with various aspect ratios. Thoracic Cancer 2010;3:116-25.
42. Hofmann W, Sturm R. Stochastic model of particle clearance in human bronchial airways. J Aerosol Med 2004;17:73-89.
43. Sturm R, Hofmann W. Mechanistic interpretation of the slow bronchial clearance phase. Radiat Prot Dosimetry 2003;105:101-4.

Cite this article as: Sturm R. Radioactivity and lung cancer-mathematical models of radionuclide deposition in the human lungs. J Thorac Dis 2011;3:231-243. DOI: 10.3978/j.issn.2072-1439.2011.04.01